



Article

Analyzing the Effect of Nano-Sized Conductive Additive Content on Cathode Electrode Performance in Sulfide All-Solid-State Lithium-Ion Batteries

Jae Hong Choi¹, Sumyeong Choi¹, Tom James Embleton¹, Kyungmok Ko¹, Kashif Saleem Saqib¹ , Jahanzaib Ali¹, Mina Jo¹, Junhyeok Hwang¹, Sungwoo Park¹, Minhu Kim¹, Mingi Hwang¹, Heesoo Lim¹ and Pilgun Oh^{1,2,*} 

¹ Department of Smart Green Technology Engineering, Pukyong National University, 45, Yongso-ro, Nam-gu, Busan 48547, Republic of Korea; critical316@naver.com (J.H.C.); csmkie9805@gmail.com (S.C.); tembleton77@gmail.com (T.J.E.); ahr17237@gmail.com (K.K.); kashifsaqib90@gmail.com (K.S.S.); jahanzaib.ali12@yahoo.com (J.A.); alskgmadl98@gmail.com (M.J.); junhyeock74@gmail.com (J.H.); tjddn8117@gmail.com (S.P.); skkim633@gmail.com (M.K.); t66549@gmail.com (M.H.); gmltn6649@naver.com (H.L.)

² Department of Nanotechnology Engineering, Pukyong National University, 45, Yongso-ro, Nam-gu, Busan 48547, Republic of Korea

* Correspondence: poh@pknu.ac.kr; Tel.: +82-51-629-6387; Fax: +82-51-629-6388

Abstract: All-solid-state lithium-ion batteries (ASSLBs) have recently received significant attention due to their exceptional energy/power densities, inherent safety, and long-term electrochemical stability. However, to achieve energy- and power-dense ASSLBs, the cathode composite electrodes require optimum ionic and electrical pathways and hence the development of electrode designs that facilitate such requirements is necessary. Among the various available conductive materials, carbon black (CB) is typically considered as a suitable carbon additive for enhancing electrode conductivity due to its affordable price and electrical-network-enhancing properties. In this study, we examined the effect of different weight percentages (wt%) of nano-sized CB as a conductive additive within a cathode composite made up of Ni-rich cathode material ($\text{LiNi}_{0.8}\text{Co}_{0.1}\text{Mn}_{0.1}\text{O}_2$) and solid electrolyte ($\text{Li}_6\text{PS}_5\text{Cl}$). Composites including 3 wt%, 5 wt%, and 7 wt% CB were produced, achieving capacity retentions of 66.1%, 65.4%, and 44.6% over 50 cycles at 0.5 C. Despite an increase in electrical conductivity of the 7 wt% CB sample, a significantly lower capacity retention was observed. This was attributed to the increased resistance at the solid electrolyte/cathode material interface, resulting from the presence of excessive CB. This study confirms that an excessive amount of nano-sized conductive material can affect the interfacial resistance between the solid electrolyte and the cathode active material, which is ultimately more important to the electrochemical performance than the electrical pathways.

Keywords: conductive additive; super C; carbon nanofiber; all-solid-state lithium batteries; morphology



Citation: Choi, J.H.; Choi, S.; Embleton, T.J.; Ko, K.; Saqib, K.S.; Ali, J.; Jo, M.; Hwang, J.; Park, S.; Kim, M.; et al. Analyzing the Effect of Nano-Sized Conductive Additive Content on Cathode Electrode Performance in Sulfide All-Solid-State Lithium-Ion Batteries. *Energies* **2024**, *17*, 109. <https://doi.org/10.3390/en17010109>

Academic Editor: Antonino S. Arico

Received: 14 November 2023

Revised: 21 December 2023

Accepted: 22 December 2023

Published: 24 December 2023



Copyright: © 2023 by the authors. Licensee MDPI, Basel, Switzerland. This article is an open access article distributed under the terms and conditions of the Creative Commons Attribution (CC BY) license (<https://creativecommons.org/licenses/by/4.0/>).

1. Introduction

Lithium-ion batteries (LIBs) have found extensive use in many modern commercial applications, ranging from portable and mid-sized electronic devices like mobile phones and laptops to larger systems like electric vehicles (EVs) and stationary energy storage units [1]. Their popularity can be attributed to their exceptional specific energy and energy density, long-lasting cycle performance, extended shelf life, and minimal self-discharge, making them suitable for diverse applications [2]. However, the technology is plagued by concerning safety issues, often arising from the use of liquid electrolytes that rely on highly volatile and flammable organic solvents. These issues are major barriers for the market expansion of LIBs, as they hinder the performance potential and limit the general adoption of EVs [3–5]. Hence, recent research is increasingly focused on all-solid-state lithium-ion batteries (ASSLBs), which not only have enhanced theoretical energy/power

densities but also address these long-term safety, and electrochemical and thermal stability issues [6,7]. The growing enthusiasm for ASSLBs research stems from the remarkable advancements made in sulfide solid electrolytes (SSEs) [7]. The development of SSEs with ion conductivities similar to those of liquid electrolytes, and in some cases even surpassing them, has been achieved [8]. ASSLBs, which comprise a cathode material, an SSE, and a high-capacity anode material have garnered considerable attention [9,10]. These batteries offer the potential for increased energy density and enhanced safety performance, making them appealing alternatives to traditional LIB systems.

This rapid shift in research towards ASSLBs underscores the desire for improved energy densities, which is further exemplified by the movement towards the application of high-capacity cathode materials [11,12]. Although LiCoO_2 cathode material initially played a pivotal role in the commercialization of LIBs, its practical capacity is limited to 140–150 mAh/g within the 3.6–4.2 V voltage range, which is significantly lower than theoretical capacity of 274 mAh/g. This comes as a result of severe structural stress at higher operating voltages [13,14]. Surface modification and bulk doping have been attempted as a means to allow for the application of higher cut-off voltages, but further research is still required before this can be effectively implemented [15]. As a result, Ni-rich layered compounds ($\text{LiNi}_{1-x-y}\text{M}_x\text{M}_y\text{O}_2$, $\text{M} = \text{Co}, \text{Mn}$) have gained the main share of attention over the past decade, highlighting a shift towards a more focused exploration of Ni-rich cathode materials [11,16].

Although the specific capacity increases with the Ni content of the cathode material, the electrical conductivity of the material decreases simultaneously [17]. Therefore, when using Ni-rich cathodes, it is crucial to design an electrode with a well-formed electron transfer network to address the limited high-power density [18]. Given that cathode materials typically have electrical conductivity in the range of approximately 10^{-5} to 10^{-6} S/cm [17], cost-effective carbon materials, valued for their affordability, low weight, and significantly superior electrical conductivity, have been introduced as conductive additives in the electrode. These carbon materials, including carbon black (CB) [16], carbon nanotubes (CNTs) [18], graphene [19], and carbon nanofibers (CNFs) [20], have been incorporated with the aim of enhancing the cathode electrode's capability to effectively manage high charging and discharging rates (Table S1).

To enhance the lithium ion conductivity of the cathode electrode in ASSLBs, 20–40 wt% micron-sized solid electrolyte (SE) is typically incorporated, while the conductive additive is kept at approximately 5 wt% to maintain suitable electrical conductivity [21]. Initially, carbon black (CB) was applied as the conductive additive in ASSLBs, partially due to its affordability [22,23]. However, recent research suggests a shift to the application of carbon nanofibers (CNFs) as the conductive additive in ASSLBs [9,10], which differs from the prevalent application of CB in LIBs. The primary reason behind this shift to using carbon nanofibers (CNFs) as a conductive additive in ASSLBs is their compatibility with SSEs, while the exact reasons for avoiding carbon black (CB) as a conductive additive in ASSLBs remain somewhat unclear. Previous research has extensively covered the interfacial reactions between the solid electrolyte and the carbon black [24,25]. Studies regarding the introduction and analysis of a variety of carbon materials have also been conducted in order to determine which structural and chemical properties of these materials are most likely to result in such reactions [26]. It was concluded that conductive material, in general, is an issue in ASSLBs and that any electron carrier degrades the solid electrolyte, regardless of the form or type of carbon applied [27–29]. These interfacial issues between CB and SSE have been fundamentally well established; however, multiple researchers have continued to use CB as a primary carbon additive material and have achieved good results through modifications of the active material [23,29–31]. Due to this continued application, further research on understanding the degradation mechanisms of cathode composites including CB is required. This can begin with gaining an understanding of the dispersion, distribution and location of the carbon black material in the cathode composite electrode and how this may affect the overall electrochemical performance.

In this study, electrodes with various weight percentages of nano-sized CB as a conductive additive were fabricated and an analysis of the electrochemical performance was conducted with a focus on the interfacial resistance. To fabricate the cathode electrode, Ni-rich cathode material ($\text{LiNi}_{0.8}\text{Co}_{0.1}\text{Mn}_{0.1}\text{O}_2$), solid electrolyte ($\text{Li}_6\text{PS}_5\text{Cl}$ argyrodite), and CB were mixed and pressed to form pellet-type electrodes. The electrodes were prepared with different CB wt% ratios, reducing the proportion of cathode materials in the composite in proportion to the increasing conductive additive content, while fixing the wt% of the solid electrolyte. The CB showed a uniform distribution throughout the electrode not only around the cathode material but also in close proximity to the solid electrolyte, as confirmed through SEM analysis. Moreover, as the wt% of CB increased (3 wt%, 5 wt%, and 7 wt%), the amount of CB distributed within the electrode naturally increased along with the proportion of CB located near the solid electrolyte. During the initial charge–discharge at 0.05 C (1 C = 200 mA/g), the discharge capacities for electrodes with 3%, 5%, and 7% CB were similar, measuring 185.4, 187.8, and 189.5 mAh/g, respectively. However, after 50 charge–discharge cycles at 0.5 C, the capacity retentions for the electrodes with 3% and 5% CB were 66.1% and 65.4%, respectively, whereas the 7% CB electrode exhibited a much lower cycle retention of 44.6%. This decrease was attributed to the increased interfacial resistance between the solid electrolyte and cathode materials during the cycling process, as confirmed through electrochemical impedance spectroscopy (EIS) analysis.

2. Experimental Materials and Methods

2.1. Synthesis of NCM811

A transition metal ion ratio of 8:1:1 (Ni:Co:Mn) was maintained, and nickel sulfate ($\text{NiSO}_4 \cdot 6\text{H}_2\text{O}$), cobalt sulfate ($\text{CoSO}_4 \cdot 7\text{H}_2\text{O}$), and manganese sulfate ($\text{MnSO}_4 \cdot 2\text{H}_2\text{O}$) were added to a deionized water solution, at a metal-ion concentration of ~ 0.56 mol/L. In a continuously stirring tank reactor (CSTR), the solution was stirred with a precipitator solution (NaOH) at concentration 1 mol/L. An ammonia solution (0.5 mol/L) buffering agent was also added continuously at this point under N_2 conditions. A pH of between 10.5 and 11.5 was maintained the entire time, with the temperature of reactor being maintained at 50°C . The reaction proceeded for 24 h until the precursor particle of $\text{Ni}_{0.8}\text{Co}_{0.1}\text{Mn}_{0.1}(\text{OH})_2$ was precipitated. The particles were washed and dried for 24 h before being mixed with $\text{LiOH} \cdot \text{H}_2\text{O}$ at a molar ratio of 1:1.03 and preheated at 500°C for 5 h to melt the lithium precursor before directly being increased to a calcination temperature of 800°C for 15 h.

2.2. Material Characterization Method

Scanning electron microscopy (SEM) TESCAN (VEGA II LSU) was used to assess the composite morphology in the backscattered electron (BSE) mode. The pellets that were analyzed using SEM were made using the standard cathode composite method outlined below, with a pellet mass of 0.05 g. This was then pressed in a hydraulic press at a pressure of 15 MPa for 12 s to form a disc-like pellet that would be structurally robust during analysis. The pellets were formed in the cell, and they were then removed intact from the cell unit before SEM analysis.

2.3. Coin Cell Fabrication Method of ASSLBs

The NCM811:SE:CA (CA = Super-C) composite ratio was altered to suit the carbon additive weight percent of the particular experiment. For the 3, 5, and 7 wt% samples, the ratios were at 70:27:3, 68:27:5, and 66:27:7, respectively. For the standard cell measurements, NCM811 (0.168 g) was weighed into a mixing mortar with LPSCl solid electrolyte (0.072 g). The samples were mixed until uniform (~ 10 min). Carbon black (Super-C) (0.024 g) was added and mixed until uniform (~ 10 min). The same mixing process was maintained despite changes in the composition.

The coin cells were made up of 0.015 g of the cathode composite outlined above as the positive electrode, a 0.15 g layer of LPSCl as the solid electrolyte separator, and 0.35 g of lithium/indium/SE (1:3.2:0.8) composite counter/reference electrode with the respective

counter electrode components being at 20 wt%, 64 wt%, and 16 wt%, respectively. The separator layer of the solid LPSCI electrolyte was pressed for 12 s at a pressure of 10 MPa in the central component of the coin cell to form a robust pellet-type separator. Positive electrode material was added to the top of the separator layer carefully, and the cathode electrode cap was placed above and twisted to ensure that the electrode material was well dispersed at the surface. The counter electrode lithium–indium anode material was added to the negative electrode side. A current collector (Ni foil) was then inserted on top of the counter electrode to protect the cell. The entire cell was pressed at 40 MPa.

2.4. Electrochemical Characterization Method

Cell cycling analysis was conducted at a standard temperature of 30 °C. The C-rate for the formation step was 0.05 C (1 C = 200 mA/g). The C-rate for the cycling steps was 0.5 C. The voltage range was maintained between 2.5 and 4.3 V vs. Li/Li⁺. The cell was allowed to reach a uniform temperature of 30 °C through resting in the battery cyler for 10 h before the analysis began.

The DC polarization analysis was conducted with a standard cathode pellet at a weight of 0.1 g after pressing at 50 MPa for 4 min. The analysis was conducted by holding the cell at a voltage of 50 mV for 1 h, followed by −50 mV for 1 h, and measuring the current throughout this time to the point where the current reached its plateau [32]. The resistance was then calculated using $V = IR$, followed by the electrical conductivity, applying methods previously outlined for calculating conductivities through pellets [33].

The electrochemical impedance spectroscopy (EIS) measurements were conducted using the standard cell set-up outlined for the galvanostatic cycling measurements, with the exact composite method and process method as outlined above. The analysis was conducted in the frequency range of 0.1 Hz to 100 kHz.

3. Result and Discussion

When fabricating the composites using nano-sized CB as a conductive additive, a constant ratio of solid electrolyte was maintained by ensuring that the total weight of the CB and NCM811 cathode material totalled 73 wt%. Accordingly, for composites containing 3, 5, and 7 wt% CB, the NCM811 cathode material was adjusted to 70, 68, and 66 wt%, while the solid electrolyte remained at 27 wt%. We prepared three type of composites, which were subsequently formed into pellets under an applied pressure of 40 MPa. The pellets were analyzed using scanning electron microscopy (SEM) in backscattered electron (BSE) mode to examine the distribution and positioning of CB within the composites. In BSE mode, heavier elements appear relatively bright, while lighter elements appear relatively dark. As a result, the cathode material appeared relatively bright, the solid electrolyte appeared relatively dark, and the carbon appeared the darkest; hence, all were clearly distinguishable. Figure 1a–c show that the conductive additives were uniformly distributed within the composites throughout the mixing process, regardless of the wt%. Furthermore, as the CB composition increased from 3 wt% to 5 wt% and 7 wt%, the area covered by CB also increased relatively. A zoomed-in view of the SEM images (Figure 1d–f) provided a clearer insight into the location of CB within the composites. We marked CB, NCM811 active material particles, and SSE particles with white, green, and orange arrows, respectively. It was evident that CB was positioned not only between NCM811 particles but also between NCM811 and SE. This can be observed clearly in the image-processed SEM images (Figure S1). Moreover, the proportion of CB adhered to the surfaces of SE and NCM811 increased with the increase in the wt% of CB. In particular, composites containing 7 wt% CB exhibited a substantial amount of CB adherence at the surface of both SE and NCM. This contact of the NCM and CB may be beneficial to the conductive network and generally works to improve the overall cell performance; however, the relatively unavoidable and simultaneous CB contact with SE is a negative factor. As discussed, the direct barrier resulting from the CB dispersion affects the ion movement from SE to NCM. Additionally, the CB, with its high relative voltage as the composite's primary

electron carrier, likely degrades the solid electrolyte and cause irreversible capacity fade. Determining the importance of these positive and negative factors by controlling the CB wt% within the composite can provide researchers with great insight into the limiting conductivity factor within cathode composites.

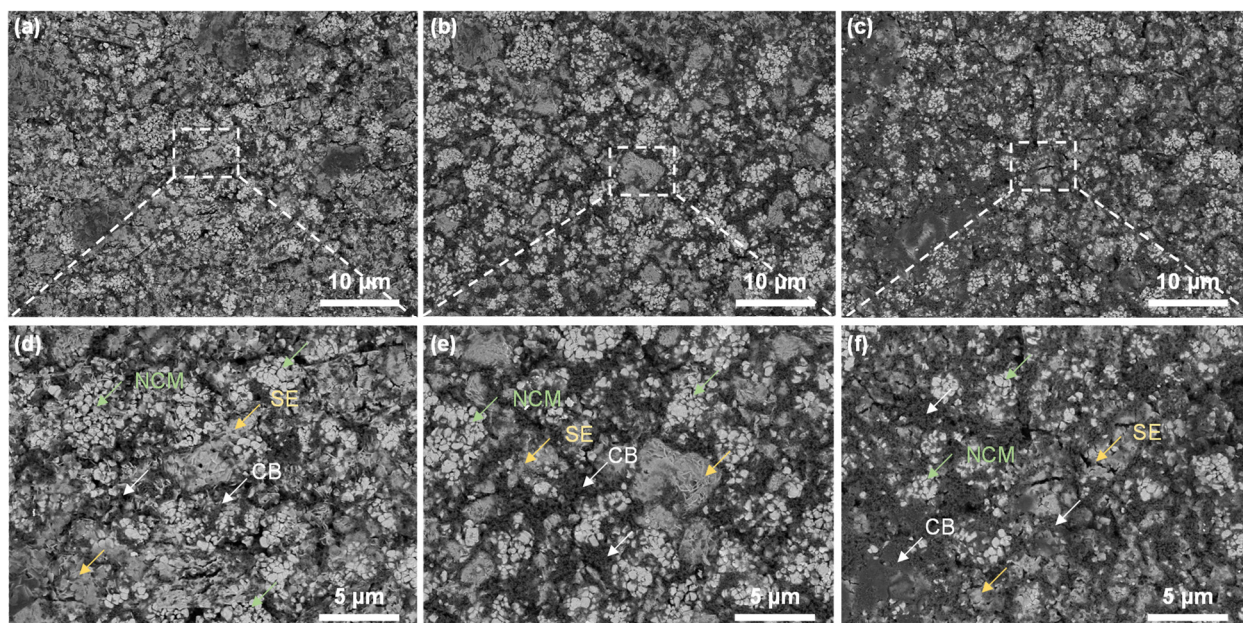


Figure 1. Scanning electron microscopy (SEM) images of the surface of (a) 3 wt%, (b) 5 wt%, and (c) 7 wt% carbon black (CB) composites after pelletizing, and the corresponding zoomed-in images of these samples (d–f), respectively.

The electrochemical properties of the three composites were evaluated in the ASSLB configuration. The composite wt% of the CB conductive additive was altered to compare the initial charge/discharge capacity and cycle performance, with $\text{LiNi}_{0.8}\text{Co}_{0.1}\text{Mn}_{0.1}\text{O}_2$ as the composite cathode material. As shown in Figure 2a, when 3 wt% CB was used as the conductive additive and the composite was charged/discharged at 0.05 C (1 C = 200 mA/g), the resulting charge capacity was 240.7 mAh/g, and the discharge capacity was 185.4 mAh/g, giving an initial Coulombic efficiency (ICE) of 77.0%. For the composite made with 5 wt% CB, the charge capacity was 234.6 mAh/g, the discharge capacity was 187.8 mAh/g, and the initial efficiency was 80.1%. In the case of the composite with 7 wt% CB, it exhibited a charge capacity of 242.9 mAh/g, a discharge capacity of 189.5 mAh/g, and an initial efficiency of 78.0%. Regardless of the wt%, the charge capacity ranged from 234 to 243 mAh/g, and the discharge capacity ranged from 185 to 189 mAh/g, showing relatively similar charge/discharge capacities at a 0.05 C rate. A sample with 0 wt% CB was also analyzed; however, the voltage was continuously unstable (Figure S2). Upon examining the zoomed-in initial charge voltage profile (Figure 2b), it was evident that the composite with 3 wt% CB reached the typical charge potential associated with the cathode material (~ 3.6 V vs. Li/Li^+) earlier along the x -axis (capacity) compared to the other composites. This initial charging capacity in the lower regions of the y -axis represents the irreversible capacity associated with the oxidation of the solid electrolyte, which appears to be related to the wt% of the CB conductive additive. These reactions in the cathode form reaction products that result in poorer cathode composite performance [28,34]. These results can be easily explained if both the electrical conductivity network and the side reactions between the CB and SE are considered. Both of these can be assumed to change as a direct result of the distribution of the CB throughout the composite. The lower ICE of the 3 wt% sample could be attributed to the electrically isolated active material due to the poor electrical network. Conversely, the lower performance of the 7 wt% sample could be attributed to the great distribution of CB within the cathode composite and to the resulting side reactions between

the CB and the SE, as shown in Figure 2b. This suggests that without the capacity attributed to the oxidation of the SE, the 5 wt% and 7 wt% composites would exhibit very similar performance, meaning that the electrical conductivity network was likely satisfied at 5 wt% CB when formations occurred at these low rates. Figure 2c shows the discharge capacity and Coulombic efficiency over 50 cycles at a charge/discharge rate of 0.5 C. In the case of the composite with 3 wt% CB, the initial cycle's discharge capacity was 145.1 mAh/g. It retained a capacity of only 95.9 mAh/g by the 50th cycle, resulting in a retention rate of 66.1% after 50 cycles, which was the highest among the tested composites. This result suggests that the high rate performance could be attributed to the ionic kinetics of the cathode composite, which would be directly related to the distribution of the CB and the associated side reactions between the CB and the solid electrolyte. Subsequently, the composite with 5 wt% CB exhibited electrochemical performance similar to that of the composite with 3 wt% CB (Table 1). This suggested that the maintenance of the ionic pathways, which is required for good cycling stability of the cell, was satisfied at 5 wt% CB. Lastly, for the composite with 7 wt% CB, the initial cycle discharge capacity was the highest among the three types at 153.5 mAh/g. However, its discharge capacity dropped to 68.4 mAh/g, resulting in the lowest retention rate of 44.6% among the three types. This suggests that low interfacial resistance is significantly more important than the electrical conductivity network. This additionally suggests that the side reactions are not the only factor affecting the kinetics of the cathode composite and that the distribution and physical barrier effects of the carbon additives are clearly playing additional roles. Table S2 further evidences this point, with the irreversible capacity of the 1st, 10th, 20th, 30th, 40th, and 50th cycles clearly showing that the irreversible capacity of these cycles followed the general trend of 7 wt% CB > 3 wt% CB > 5 wt% CB. This verified that a certain portion of the irreversible capacity observed in the 3 wt% sample arose from the electrical isolation of the active material, whereas the 7 wt% sample likely owed its greater irreversible capacity to capacity lost to side reactions with the SE and the distribution of CB within the cathode composite. Interestingly, the 5 wt% sample appeared to have the lowest irreversible capacity and hence the highest coulombic efficiency at the selected cycles, and to have good electrical conductivity and few interfacial reactions with the SE.

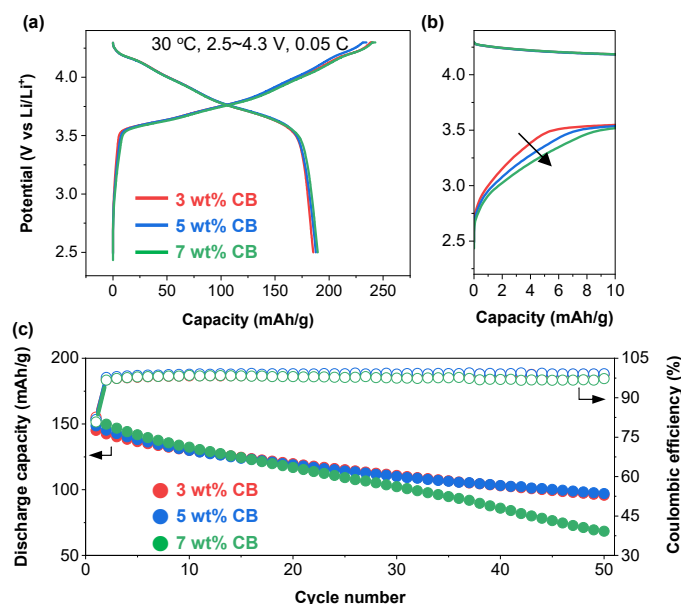


Figure 2. (a) Electrochemical performance of 3 wt%, 5 wt%, and 7 wt% CB composites for the formation (initial charge–discharge) voltage profiles in the voltage range of 2.5–4.3 V at 0.05 C; (b) zoomed-in initial voltage profiles at 0.05 C (c) following cycle performance and coulombic efficiency at 0.5 C.

Table 1. Initial charge–discharge capacities and initial coulombic efficiencies (ICEs) of 3 wt%, 5 wt%, and 7 wt% CB composites conducted at 0.05 C. Cycle charge and discharge capacities of the 1st and 50th cycles and capacity retentions over 50 cycles conducted at 0.5 C.

	Charge Capacity (mAh/g)	Discharge Capacity (mAh/g)	ICE (%)	Discharge Capacity @ 1st (mAh/g)	Discharge Capacity @ 50th (mAh/g)	Capacity Retention @ 50th (%)
3 wt% CB	240.7	185.4	77.0	145.1	95.9	66.1
5 wt% CB	234.6	187.8	80.1	148.6	97.1	65.4
7 wt% CB	242.9	189.5	78.0	153.5	68.4	44.6

When manufacturing these composites, an equal amount of solid electrolyte was used in all three composites, ensuring similar ionic conductivity within the composites. However, the composite with 7 wt% CB showed the lowest retention rate despite it having superior electrical conductivity due to having the highest carbon additive content. When conducting potentiostatic measurements using ion-blocking electrodes on either side, the electrical conductivities for each of these composites were $11.94 \times 10^{-3} \text{ S cm}^{-1}$, $16.4 \times 10^{-3} \text{ S cm}^{-1}$, and $20.94 \times 10^{-3} \text{ S cm}^{-1}$, respectively (Figure 3a,b). As expected, the composite with 7 wt% CB exhibited the highest electrical conductivity. Despite having high electrical conductivity, the lower cycling performance suggested that an excessive amount of the conductive additive may obstruct lithium-ion pathways, resulting in decreased ionic conductivity and, consequently, reduced overall performance. This approach aligns with the analysis from the SEM images in Figure 1, where an excessive amount of carbon additive was observed to be located between the solid electrolyte and cathode materials, potentially hindering ionic movement across the interface.

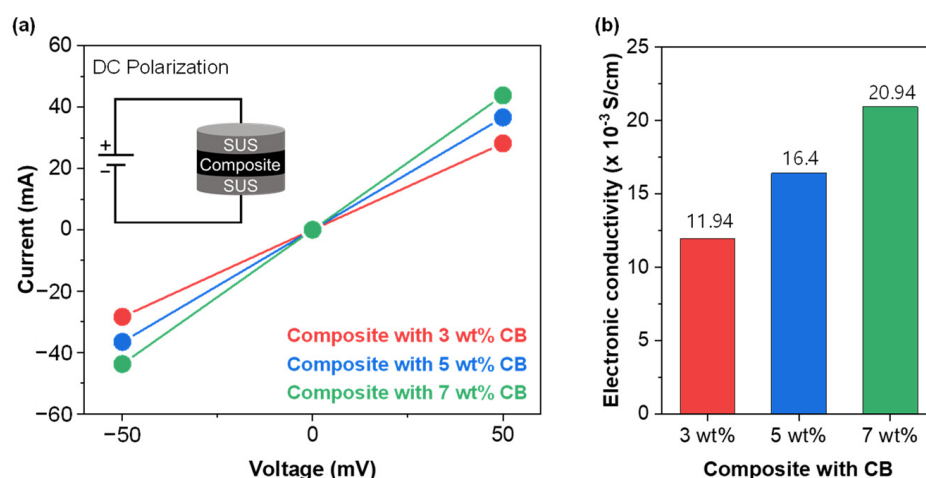


Figure 3. (a) DC polarization (I–V analysis) at 30 °C and (b) calculated electronic conductivity of composite with 3, 5, and 7 wt% of CB.

To evaluate the influence of conductive additives on the impedance between the cathode electrode and solid electrolytes (SEs) during charge–discharge cycles, electrochemical impedance spectroscopy (EIS) tests on composites with 3, 5, and 7 wt% CB were conducted. These tests were conducted both immediately after the formation cycle (Figure S3, Table S3) and after 50 cycles (Figure 4), as is common practice in previous research [35–37]. The Nyquist plots display semicircles observed at high frequencies (HFs) and intermediate frequencies (IFs) and a line at low frequencies (LFs), corresponding to the impedance of the solid electrolyte interface (R_{GB}), the interfacial and charge transfer impedance between the cathode materials and solid electrolyte (R_{CT+SEI}), and the Warburg impedance, respectively [38]. The intersection of the high-frequency curve with the Z_{re} axis indicates the bulk impedance (R_{bulk}) of the solid electrolyte [39,40]. The R_{bulk} values of the composites with 3, 5, and 7 wt% CB were 27.41 Ω , 33.90 Ω , and 43.25 Ω after 50 cycles, respectively (Figure 4).

This corresponds to a fairly consistent increase from the 3 wt% sample to the 5 wt% and 7 wt% samples. This indicates that the overall lithium ion conductivity of the SEs in the composite changes over cycling, confirming that the introduction of greater amounts of CB results in greater side reactions with the SE and causes high-resistance compound formation [41,42]. The R_{CT+SEI} values of the composites made with 3, 5, and 7 wt% of CB were 250.8 Ω , 286.8 Ω , and 399.5 Ω , respectively, after 50 cycles. As the wt% of CB increased, the interfacial resistance also increased (Table 2). Considering the analysis of the composite morphology from the SEM analysis in Figure 1, it was determined that an excessive amount of nano-sized conductive additives within the composite tended to be located between SE and cathode materials, leading to an increase in interfacial resistance. Additionally, an increase in the solid electrolyte interface layer, due to the side reactions between the CB and the solid electrolyte, was attributed to the interfacial resistance encompassed by R_{CT+SEI} .

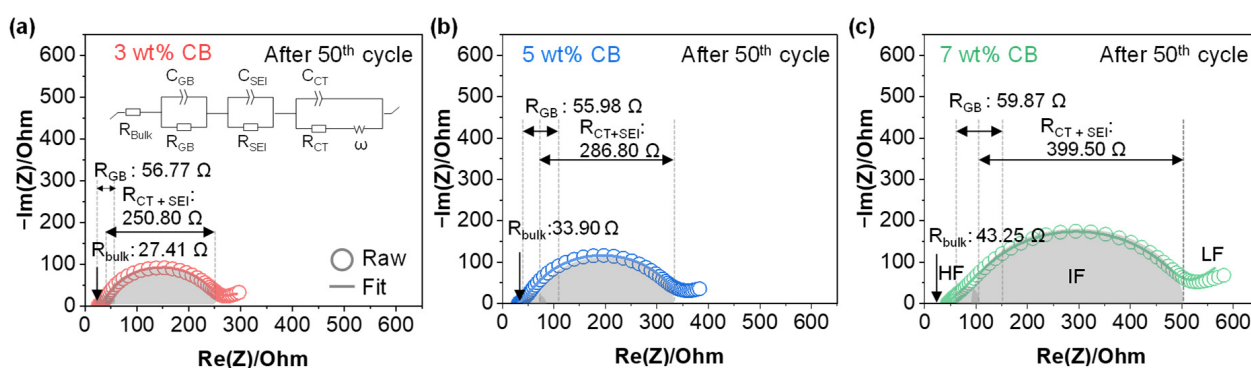


Figure 4. Nyquist plots (0.1 Hz–100 kHz) and their fittings for (a) 3 wt%, (b) 5 wt%, and (c) 7 wt% CB composites comparing results obtained after 50 cycles at 0.5 C.

Table 2. Solid electrolyte bulk resistance (R_b), cathode electrolyte interphase resistance (R_{GB}), and charge transfer resistance (R_{CT}) of 3 wt%, 5 wt%, and 7 wt% CB composites after the 50th cycle at 0.5 C determined via electrochemical impedance spectroscopy (EIS).

	Sample	R_{bulk} (Ω)	R_{GB} (Ω)	R_{CT+SEI} (Ω)
After 50th cycle	3 wt% CB	27.4	56.8	250.8
	5 wt% CB	33.9	56.0	286.8
	7 wt% CB	43.3	59.9	399.5

To investigate the difference in cycling performance attributed to the increased interfacial resistance at the SE–cathode interface, the 0.5 C charge–discharge profiles were examined. Among the composites with 3 and 5 wt% CB, the cycle evaluation profiles appeared relatively similar (Figure 5a,b), whereas the composites fabricated with 7 wt% CB exhibited distinctive variations in the profile (Figure 5c). The composite with 7 wt% CB showed a distinguishably larger polarization at the initial point of discharge and exhibited larger overpotential during the cycling compared to those composites prepared with 3 or 5 wt% CB, as indicated by the long constant-voltage (CV) charge stage. This long CV stage is typically associated with large internal resistance, which can be attributed to electrical network or large ionic interfacial resistance [21,43]. This long CV state typically corresponds to a poor CE, as evidenced in Table S2, with 3 wt% CB, 5 wt% CB, and 7 wt% CB having average CEs of 95.95%, 96.15%, and 94.68%, respectively. Additionally, the IR drop exhibited at the point of discharge can also be a significant indicator of increased internal resistance in the charged state [44,45]. Since the 7 wt% CB cell had the most conductive additive present in the cathode composite, it is unlikely that this would have occurred due to a large electrical resistance, so it is more likely that this could be attributed to ionic resistance arising from the distribution of the CB and the degraded solid electrolyte. The increased interfacial resistance caused by the positioning of CB between the SE and cathode

materials evidently accelerated cell degradation, particularly at the higher C-rate where ionic conductivity becomes a major limitation [46].

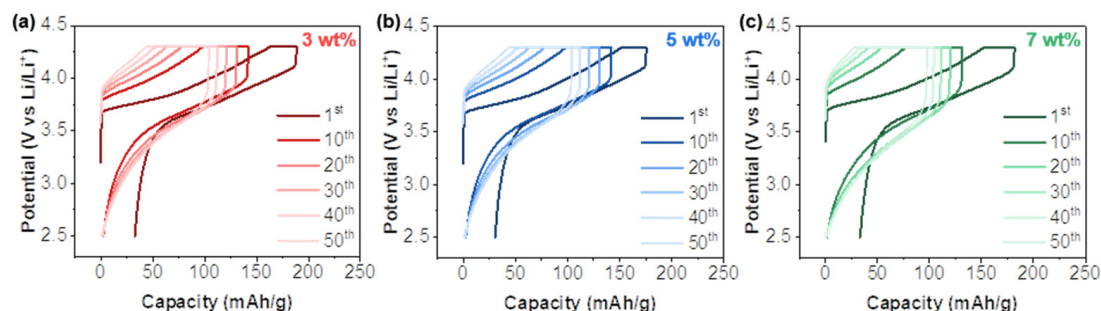


Figure 5. Charge–discharge voltage profiles of composites with (a) 3 wt%, (b) 5 wt%, and (c) 7 wt% CB at 0.5 C cycling in the voltage range of 2.5–4.3 V at 30 °C. The curves were created using the rate data in Figure 2c.

4. Conclusions

In conclusion, this study examined the distribution of a nano-sized conductive material, CB, within the ASSLB cathode composite and assessed the electrochemical performance by altering the CB ratio in the composite. Composites with 3, 5, and 7 wt% of CB were considered, along with 70%, 68%, and 66% of the cathode materials, respectively. In all cases, the total weight percentage of the conductive materials and cathode materials remained at 73%, with the remaining 27% was composed of solid electrolyte. The results of electrochemical analysis indicated that composites with 3% and 5% CB exhibited similar electrochemical performance. However, the composite containing 7% CB exhibited a noticeable decline in cycle stability over 50 cycles. Although the increase in CB content, in the case of the composite with 7 wt% CB, led to enhanced electrical conductivity in the composite, it also resulted in a higher quantity of CB situated between the SE and cathode active materials, thereby increasing the interfacial resistance at the SE–cathode interface (Figures 6 and S4). As a result, significant overpotential and polarization were observed during the 50-cycle charge–discharge process. These findings suggest that an excessive amount of nano-sized CB conductive material can affect the interfacial resistance between the SE and cathode active material, ultimately leading to a decrease in electrical performance.

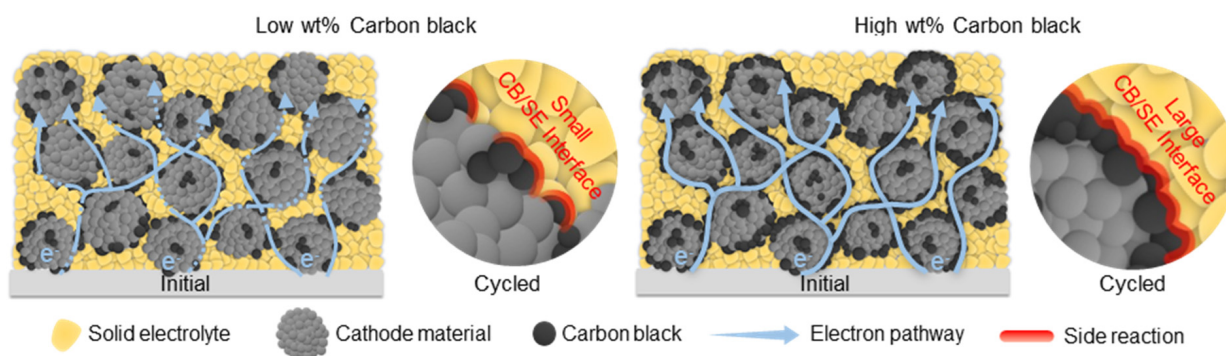


Figure 6. Scheme of the electrical conductivity of the cathode electrode and ionic resistance between cathode materials and solid electrolyte after fabricating a composite using nano-sized carbon black as a conductive material.

Supplementary Materials: The following supporting information can be downloaded at: <https://www.mdpi.com/article/10.3390/en17010109/s1>, Figure S1: Scanning Electron Microscopy (SEM) images of the surface of (a) 3 wt%, (b) 5 wt% and (c) 7 wt% carbon black (CB) composites after pelletizing with the look-up table (LUT) color gradient altered to better display the 3 components of the cathode composite; Figure S2: Electrochemical performance of 0 wt% CB composite for the formation (initial charge-discharge) voltage profiles in the voltage range of 2.5–4.3 V at 0.05 C; Figure S3: Nyquist plots (0.1 Hz – 100 kHz) and their fittings for (a) 3 wt%, (b) 5 wt%, and (c) 7 wt% CB composites comparing results obtained after formation at 0.05 C; Figure S4: Scheme weighing the importance of electrical conductivity of the cathode electrode and the corresponding interfacial resistance between carbon materials and solid electrolyte from inclusion of 3 wt%, 5 wt%, and 7 wt% CB, Table S1: Table highlighting the properties and impact of applying of various carbon additives, as characterized by previous work, Table S2: The charge-discharge capacities, the irreversible capacities, and coulombic efficiencies (CE) of 3 wt%, 5 wt%, and 7 wt% CB composites conducted at 0.5 C for the 1st, 10th, 20th, 30th, 40th, and 50th cycles, Table S3: Solid electrolyte bulk resistance (R_b), cathode electrolyte interphase resistance (R_{GB}), and charge transfer resistance (RCT) of 3 wt%, 5 wt%, and 7 wt% CB composites after formation at 0.05 C determined via Electrochemical Impedance Spectroscopy (EIS).

Author Contributions: Methodology, S.C., K.K. and S.P.; Investigation, K.S.S., J.A., M.K. and H.L.; Data curation, M.J., J.H. and M.H.; Writing—review & editing, J.H.C. and T.J.E.; Supervision, P.O. All authors have read and agreed to the published version of the manuscript.

Funding: This work was supported by the Basic Science Research Program through the National Research Foundation of Korea (NRF) funded by the Ministry of Education (2022R111A3069172) and was supported by a Korea Institute of Energy Technology Evaluation and Planning (KETEP) grant funded by the Korea government (MOTIE) (20221B1010003B, Integrated High-Quality Technology Development of Remanufacturing Spent Cathode for Low Carbon Resource Recirculation), supported by “Regional Innovation Strategy (RIS)” through the National Research Foundation of Korea (NRF) funded by the Ministry of Education (MOE) (2023RIS-007).

Data Availability Statement: Data is contained within the article and supplementary material.

Conflicts of Interest: The authors declare no conflict of interest.

References

1. Blomgren, G.E. The Development and Future of Lithium ion Batteries. *J. Electrochem. Soc.* **2016**, *164*, A5019. [[CrossRef](#)]
2. Kang, Y.; Deng, C.; Chen, Y.; Liu, X.; Liang, Z.; Li, T.; Hu, Q.; Zhao, Y. Binder-free Electrodes and their Application for Li-ion Batteries. *Nanoscale Res. Lett.* **2020**, *15*, 112. [[CrossRef](#)] [[PubMed](#)]
3. Love, C.T.; Buesser, C.; Johannes, M.D.; Swider-Lyons, K.E. Innovating Safe Lithium-ion Batteries Through Basic to Applied Research. *J. Electrochem. Energy Convers. Storage* **2018**, *15*, 011006. [[CrossRef](#)]
4. Finegan, D.P.; Darcy, E.; Keyser, M.; Tjaden, B.; Heenan, T.M.; Jervis, R.; Bailey, J.J.; Vo, N.T.; Magdysyuk, O.V.; Drakopoulos, M. Identifying the Cause of Rupture of Li-Ion Batteries During Thermal Runaway. *Adv. Sci.* **2018**, *5*, 1700369. [[CrossRef](#)] [[PubMed](#)]
5. Chen, Y.; Kang, Y.; Zhao, Y.; Wang, L.; Liu, J.; Li, Y.; Liang, Z.; He, X.; Li, X.; Tavajohi, N. A Review of Lithium-ion Battery Safety Concerns: The Issues, Strategies, and Testing Standards. *J. Energy Chem.* **2021**, *59*, 83–99. [[CrossRef](#)]
6. Sun, C.; Liu, J.; Gong, Y.; Wilkinson, D.P.; Zhang, J. Recent Advances in All-solid-state Rechargeable Lithium Batteries. *Nano Energy* **2017**, *33*, 363–386. [[CrossRef](#)]
7. Zheng, Y.; Yao, Y.; Ou, J.; Li, M.; Luo, D.; Dou, H.; Li, Z.; Amine, K.; Yu, A.; Chen, Z. A Review of Composite Solid-state Electrolytes for Lithium Batteries: Fundamentals, Key Materials and Advanced Structures. *Chem. Soc. Rev.* **2020**, *49*, 8790–8839. [[CrossRef](#)]
8. Miura, A.; Rosero-Navarro, N.C.; Sakuda, A.; Tadanaga, K.; Phuc, N.H.; Matsuda, A.; Machida, N.; Hayashi, A.; Tatsumisago, M. Liquid-phase Syntheses of Sulfide Electrolytes for All-solid-state Lithium Battery. *Nat. Rev. Chem.* **2019**, *3*, 189–198. [[CrossRef](#)]
9. Lee, Y.-G.; Fujiki, S.; Jung, C.; Suzuki, N.; Yashiro, N.; Omoda, R.; Ko, D.-S.; Shiratsuchi, T.; Sugimoto, T.; Ryu, S. High-energy Long-cycling All-solid-state Lithium Metal Batteries Enabled by Silver-carbon Composite Anodes. *Nat. Energy* **2020**, *5*, 299–308. [[CrossRef](#)]
10. Tan, D.H.; Chen, Y.-T.; Yang, H.; Bao, W.; Sreenarayanan, B.; Doux, J.-M.; Li, W.; Lu, B.; Ham, S.-Y.; Sayahpour, B. Carbon-free High-loading Silicon Anodes Enabled by Sulfide Solid Electrolytes. *Science* **2021**, *373*, 1494–1499. [[CrossRef](#)]
11. Park, N.-Y.; Park, G.-T.; Kim, S.-B.; Jung, W.; Park, B.-C.; Sun, Y.-K. Degradation Mechanism of Ni-rich Cathode Materials: Focusing on Particle Interior. *ACS Energy Lett.* **2022**, *7*, 2362–2369. [[CrossRef](#)]
12. Zhang, S.S. Problems and their Origins of Ni-rich Layered Oxide Cathode Materials. *Energy Stor. Mater.* **2020**, *24*, 247–254. [[CrossRef](#)]

13. Julien, C.M.; Mauger, A.; Zaghbi, K.; Groult, H. Comparative Issues of Cathode Materials for Li-ion Batteries. *Inorganics* **2014**, *2*, 132–154. [[CrossRef](#)]
14. Voronina, N.; Sun, Y.-K.; Myung, S.-T. Co-free Layered Cathode Materials for High Energy Density Lithium-ion Batteries. *ACS Energy Lett.* **2020**, *5*, 1814–1824. [[CrossRef](#)]
15. Oh, P.; Yun, J.; Choi, J.H.; Nam, G.; Park, S.; Embleton, T.J.; Yoon, M.; Joo, S.H.; Kim, S.H.; Jang, H. New Ion Substitution Method to Enhance Electrochemical Reversibility of Co-Rich Layered Materials for Li-Ion Batteries. *Adv. Energy Mater.* **2023**, *13*, 2202237. [[CrossRef](#)]
16. Choi, J.H.; Lee, C.; Park, S.; Hwang, M.; Embleton, T.J.; Ko, K.; Jo, M.; Saqib, K.S.; Yun, J.; Jo, M. Improved Electrochemical Performance Using Well-dispersed Carbon Nanotubes as Conductive Additive in the Ni-rich Positive Electrode of Lithium-ion Batteries. *Electrochem. Commun.* **2023**, *146*, 107419. [[CrossRef](#)]
17. Amin, R.; Chiang, Y.-M. Characterization of Electronic and Ionic Transport in $\text{Li}_{1-x}\text{Mi}_{0.33}\text{Mn}_{0.33}\text{Co}_{0.33}\text{O}_2$ (NMC333) and $\text{Li}_{1-x}\text{Ni}_{0.50}\text{Mn}_{0.20}\text{Co}_{0.30}\text{O}_2$ (NMC523) as a Function of Li Content. *J. Electrochem. Soc.* **2016**, *163*, A1512. [[CrossRef](#)]
18. Choi, J.; Lee, C.; Park, S.; Embleton, T.J.; Ko, K.; Jo, M.; Saleem Saqib, K.; Yun, J.; Jo, M.; Son, Y. Analysis of Electrochemical Performance with Dispersion Degree of CNTs in Electrode According to Ultrasonication Process and Slurry Viscosity for Lithium-Ion Battery. *Nanomaterials* **2022**, *12*, 4271. [[CrossRef](#)]
19. Liu, T.; Sun, S.; Zang, Z.; Li, X.; Sun, X.; Cao, F.; Wu, J. Effects of Graphene with Different Sizes as Conductive Additives on the Electrochemical Performance of a LiFePO_4 Cathode. *RSC Adv.* **2017**, *7*, 20882–20887. [[CrossRef](#)]
20. Liu, M.; Zhang, P.; Qu, Z.; Yan, Y.; Lai, C.; Liu, T.; Zhang, S. Conductive Carbon Nanofiber Interpenetrated Graphene Architecture for Ultra-stable Sodium ion Battery. *Nat. Commun.* **2019**, *10*, 3917. [[CrossRef](#)]
21. Embleton, T.J.; Yun, J.; Choi, J.H.; Kim, J.; Ko, K.; Kim, J.; Son, Y.; Oh, P. Lithium-enhanced Functionalized Carbon Nanofibers as a Mixed Electronic/Ionic Conductor for Sulfide All Solid-state Batteries. *Appl. Surf. Sci.* **2023**, *610*, 155490. [[CrossRef](#)]
22. Xiao, Y.; Miara, L.J.; Wang, Y.; Ceder, G. Computational Screening of Cathode Coatings for Solid-state Batteries. *Joule* **2019**, *3*, 1252–1275. [[CrossRef](#)]
23. Doerrler, C.; Capone, I.; Narayanan, S.; Liu, J.; Grovenor, C.R.; Pasta, M.; Grant, P.S. High Energy Density Single-Crystal NMC/ $\text{Li}_6\text{PS}_5\text{Cl}$ Cathodes for All-solid-state Lithium-metal Batteries. *ACS Appl. Mater. Interfaces* **2021**, *13*, 37809–37815. [[CrossRef](#)] [[PubMed](#)]
24. Tan, D.H.S.; Wu, E.A.; Nguyen, H.; Chen, Z.; Marple, M.A.T.; Doux, J.-M.; Wang, X.; Yang, H.; Banerjee, A.; Meng, Y.S. Elucidating Reversible Electrochemical Redox of $\text{Li}_6\text{PS}_5\text{Cl}$ Solid Electrolyte. *ACS Energy Lett.* **2019**, *4*, 2418–2427. [[CrossRef](#)]
25. Yoon, K.; Kim, J.-J.; Seong, W.M.; Lee, M.H.; Kang, K. Investigation on the Interface Between $\text{Li}_{10}\text{GeP}_2\text{S}_{12}$ Electrolyte and Carbon Conductive Agents in All-solid-state Lithium Battery. *Sci. Rep.* **2018**, *8*, 8066. [[CrossRef](#)] [[PubMed](#)]
26. Zhang, W.; Leichtweiß, T.; Culver, S.P.; Koerver, R.; Das, D.; Weber, D.A.; Zeier, W.G.; Janek, J. The Detrimental Effects of Carbon Additives in $\text{Li}_{10}\text{GeP}_2\text{S}_{12}$ -based Solid-state Batteries. *ACS Appl. Mater. Interfaces* **2017**, *9*, 35888–35896. [[CrossRef](#)] [[PubMed](#)]
27. Quemin, E.; Dugas, R.; Koç, T.; Hennequart, B.; Chometon, R.; Tarascon, J.-M. Decoupling Parasitic Reactions at the Positive Electrode Interfaces in Argyrodite-Based Systems. *ACS Appl. Mater. Interfaces* **2022**, *14*, 49284–49294. [[CrossRef](#)]
28. Walther, F.; Randau, S.; Schneider, Y.; Sann, J.; Rohnke, M.; Richter, F.H.; Zeier, W.G.; Janek, J. Influence of Carbon Additives on the Decomposition Pathways in Cathodes of Lithium Thiophosphate-Based All-Solid-State Batteries. *Chem. Mater.* **2020**, *32*, 6123–6136. [[CrossRef](#)]
29. Zhang, J.; Zhong, H.; Zheng, C.; Xia, Y.; Liang, C.; Huang, H.; Gan, Y.; Tao, X.; Zhang, W. All-solid-state Batteries with Slurry Coated $\text{LiNi}_{0.8}\text{Co}_{0.1}\text{Mn}_{0.1}\text{O}_2$ Composite Cathode and $\text{Li}_6\text{PS}_5\text{Cl}$ Electrolyte: Effect of Binder Content. *J. Power Sources* **2018**, *391*, 73–79. [[CrossRef](#)]
30. Xia, Y.; Li, J.; Zhang, J.; Zhou, X.; Huang, H.; He, X.; Gan, Y.; Xiao, Z.; Zhang, W. Yttrium Stabilized Argyrodite Solid Electrolyte with Enhanced Ionic Conductivity and Interfacial Stability for All-solid-state Batteries. *J. Power Sources* **2022**, *543*, 231846. [[CrossRef](#)]
31. Ye, Q.; Li, X.; Zhang, W.; Xia, Y.; He, X.; Huang, H.; Gan, Y.; Xia, X.; Zhang, J. Slurry-Coated $\text{LiNi}_{0.8}\text{Co}_{0.1}\text{Mn}_{0.1}\text{O}_2$ - Li_3InCl_6 Composite Cathode with Enhanced Interfacial Stability for Sulfide-Based All-Solid-State Batteries. *ACS Appl. Mater. Interfaces* **2023**, *15*, 18878–18888. [[CrossRef](#)] [[PubMed](#)]
32. Wang, S.; Yan, M.; Li, Y.; Vinado, C.; Yang, J. Separating Electronic and Ionic Conductivity in Mix-conducting Layered Lithium Transition-Metal Oxides. *J. Power Sources* **2018**, *393*, 75–82. [[CrossRef](#)]
33. Uddin, M.-J.; Cho, S.-J. Reassessing the Bulk Ionic Conductivity of Solid-state Electrolytes. *Sustain. Energy Fuels* **2018**, *2*, 1458–1462. [[CrossRef](#)]
34. Zuo, T.-T.; Walther, F.; Ahmed, S.; Rueß, R.; Hertle, J.; Mogwitz, B.; Volz, K.; Janek, J. Formation of an Artificial Cathode–Electrolyte Interphase to Suppress Interfacial Degradation of Ni-Rich Cathode Active Material with Sulfide Electrolytes for Solid-State Batteries. *ACS Energy Lett.* **2023**, *8*, 1322–1329. [[CrossRef](#)]
35. Wang, S.; Zhang, W.; Chen, X.; Das, D.; Ruess, R.; Gautam, A.; Walther, F.; Ohno, S.; Koerver, R.; Zhang, Q.; et al. Influence of Crystallinity of Lithium Thiophosphate Solid Electrolytes on the Performance of Solid-State Batteries. *Adv. Energy Mater.* **2021**, *11*, 2100654. [[CrossRef](#)]
36. Oh, G.; Hirayama, M.; Kwon, O.; Suzuki, K.; Kanno, R. Bulk-Type All Solid-State Batteries with 5 V Class $\text{LiNi}_{0.5}\text{Mn}_{1.5}\text{O}_4$ Cathode and $\text{Li}_{10}\text{GeP}_2\text{S}_{12}$ Solid Electrolyte. *Chem. Mater.* **2016**, *28*, 2634–2640. [[CrossRef](#)]

37. Li, B.; Sun, Z.; Lv, N.; Hu, Y.; Jiang, L.; Zhang, Z.; Liu, F. Dual Protection of a Li–Ag Alloy Anode for All-Solid-State Lithium Metal Batteries with the Argyrodite $\text{Li}_6\text{PS}_5\text{Cl}$ Solid Electrolyte. *ACS Appl. Mater. Interfaces* **2022**, *14*, 37738–37746. [[CrossRef](#)]
38. Li, X.; Jin, L.; Song, D.; Zhang, H.; Shi, X.; Wang, Z.; Zhang, L.; Zhu, L. LiNbO_3 -coated $\text{LiNi}_{0.8}\text{Co}_{0.1}\text{Mn}_{0.1}\text{O}_2$ Cathode With High Discharge Capacity and Rate Performance for All-solid-state Lithium Battery. *J. Energy Chem.* **2020**, *40*, 39–45. [[CrossRef](#)]
39. Ito, S.; Fujiki, S.; Yamada, T.; Aihara, Y.; Park, Y.; Kim, T.Y.; Baek, S.-W.; Lee, J.-M.; Doo, S.; Machida, N. A Rocking Chair Type All-solid-state Lithium ion Battery Adopting Li_2O – ZrO_2 Coated $\text{LiNi}_{0.8}\text{Co}_{0.15}\text{Al}_{0.05}\text{O}_2$ and a Sulfide Based Electrolyte. *J. Power Sources* **2014**, *248*, 943–950. [[CrossRef](#)]
40. Zhang, Z.; Chen, S.; Yang, J.; Wang, J.; Yao, L.; Yao, X.; Cui, P.; Xu, X. Interface Re-engineering of $\text{Li}_{10}\text{GeP}_2\text{S}_{12}$ Electrolyte and Lithium Anode for All-solid-state Lithium Batteries with Ultralong Cycle Life. *ACS Appl. Mater. Interfaces* **2018**, *10*, 2556–2565. [[CrossRef](#)]
41. Swamy, T.; Chen, X.; Chiang, Y.-M. Electrochemical Redox Behavior of Li Ion Conducting Sulfide Solid Electrolytes. *Chem. Mater.* **2019**, *31*, 707–713. [[CrossRef](#)]
42. Han, F.; Zhu, Y.; He, X.; Mo, Y.; Wang, C. Electrochemical Stability of $\text{Li}_{10}\text{GeP}_2\text{S}_{12}$ and $\text{Li}_7\text{La}_3\text{Zr}_2\text{O}_{12}$ Solid Electrolytes. *Adv. Energy Mater.* **2016**, *6*, 1501590. [[CrossRef](#)]
43. Nara, H.; Mukoyama, D.; Shimizu, R.; Momma, T.; Osaka, T. Systematic Analysis of Interfacial Resistance Between the Cathode Layer and the Current Collector in Lithium-ion Batteries by Electrochemical Impedance Spectroscopy. *J. Power Sources* **2019**, *409*, 139–147. [[CrossRef](#)]
44. Xu, L.; Tang, S.; Cheng, Y.; Wang, K.; Liang, J.; Liu, C.; Cao, Y.-C.; Wei, F.; Mai, L. Interfaces in Solid-State Lithium Batteries. *Joule* **2018**, *2*, 1991–2015. [[CrossRef](#)]
45. Luntz, A.C.; Voss, J.; Reuter, K. Interfacial Challenges in Solid-State Li Ion Batteries. *J. Phys. Chem. Lett.* **2015**, *6*, 4599–4604. [[CrossRef](#)]
46. Wang, L.; Liu, D.; Huang, T.; Geng, Z.; Yu, A. Reducing Interfacial Resistance of a $\text{Li}_{1.5}\text{Al}_{0.5}\text{Ge}_{1.5}(\text{PO}_4)_3$ Solid Electrolyte/Electrode Interface by Polymer Interlayer Protection. *RSC Adv.* **2020**, *10*, 10038–10045. [[CrossRef](#)]

Disclaimer/Publisher’s Note: The statements, opinions and data contained in all publications are solely those of the individual author(s) and contributor(s) and not of MDPI and/or the editor(s). MDPI and/or the editor(s) disclaim responsibility for any injury to people or property resulting from any ideas, methods, instructions or products referred to in the content.